Since January 2020 Elsevier has created a COVID-19 resource centre with free information in English and Mandarin on the novel coronavirus COVID-19. The COVID-19 resource centre is hosted on Elsevier Connect, the company's public news and information website.

Elsevier hereby grants permission to make all its COVID-19-related research that is available on the COVID-19 resource centre - including this research content - immediately available in PubMed Central and other publicly funded repositories, such as the WHO COVID database with rights for unrestricted research re-use and analyses in any form or by any means with acknowledgement of the original source. These permissions are granted for free by Elsevier for as long as the COVID-19 resource centre remains active.

Chemical Engineering Journal 420 (2021) 127655

Contents lists available at ScienceDirect

Chemical Engineering Journal

journal homepage: www.elsevier.com/locate/cej

Sustainable and fast saliva-based COVID-19 virus diagnosis kit using a novel GO-decorated Au/FBG sensor

Alireza Samavati [a,b,*], Zahra Samavati [a], M. Velashjerdi [b], Ahmad Fauzi Ismail [a,*], M.H. D. Othman [a], G. Eisaabadi B [b], Mohd Sohaimi Abdullah [a], Marzieh Bolurian [c], Mohammadreza Bolurian [d]

[a] Advanced Membrane Technology Research Centre, Universiti Teknologi Malaysia (UTM), 81310 Johor Bahru, Malaysia
[b] Department of Materials Science and Engineering, Faculty of Engineering, Arak University, Arak 38156-8-8349, Iran
[c] Intensive Care Unit, Department of Infection Disease, Sina Hospital, 6517838695 Hamadan, Iran
[d] Department of Physical Education, Faculty of Humanities and Social Sciences, University of Kurdistan, 66177-15175 Sanandaj, Iran

ARTICLE INFO

Keywords:
Fiber Bragg grating sensor
Graphene oxide
COVID-19 diagnosis
Surface plasmon resonance

ABSTRACT

Monitoring the COVID-19 virus through patients' saliva is a favorable non-invasive specimen for diagnosis and infection control. In this study, salivary samples of COVID-19 patients collected from 6 patients with the median age of 58.5 years, ranging from 34 to 72 years (2 females and 4 males) were analyzed using an Au/fiber Bragg grating (FBG) probe decorated with GO. The probe measures the prevalence of positivity in saliva and the association between the virus density and changes to sensing elements. When the probe is immersed in patients' saliva, deviation of the detected light wavelength and intensity from healthy saliva indicate the presence of the virus and confirms infection. For a patient in the hyperinflammatory phase of desease, who has virus density of 1.2×10^8 copies/mL in saliva, the maximum wavelength shift and intensity changes after 1600 s were shown to be 1.12 nm and 2.01 dB, respectively. While for a patient in the early infection phase with 1.6×10^3 copies/mL, these values were 0.98 nm and 1.32 dB. The precise and highly sensitive FBG probe proposed in this study was found a reliable tool for quick detection of the COVID-19 virus within 10 s after exposure to patients' saliva in any stage of the disease.

1. Introduction

A novel coronavirus has been dispersed from the Hubei province in China, since December 2019, and has reached many countries worldwide. This virus, named as SARS-CoV-2 [1], causes the disease COVID-19, and in many countries, it is still spreading at high speed [2]. It is an enveloped, single-stranded RNA virus with high mutation and recombination rates [3]. Typically, spreading the small droplets of coughs, saliva, or exhales of COVID-19 patients is the main cause of the virus distribution. As saliva can act as an infection transmission object between individuals via contact with its spread droplets, it can be used as a reliable, convenient, and non-invasive analyte for the laboratory diagnosis of infections caused by SARS-CoV-2 as an acute respiratory syndrome [4]. Additionally, using saliva for virus diagnosis reduces the risk of infection to the healthcare workers due to the possibility of self-collecting by the patients. Saliva samples present an adequate quantity of analyte for the patients who have insufficient sputum. The existence of the SARS-CoV virus in patients' saliva has been confirmed previously, and it is reported that its quantity is approximately equal to the levels found in nasopharyngeal specimens [5]. The COVID-19 virus in saliva originated from the following sources: (1) the gingival crevicular fluid, (2) salivary glands via the ducts, and (3) the lower and upper respiratory tract secretions that are mixed with saliva [5].

For viral infection diagnosis, there are two alternative approaches: 1) serological investigations for measuring the elevated biomarker levels, and 2) direct determination of the virus through the unique structure of its cellular proteins. The use of the first approach (which is an immune-sensing one) is restricted due to the concentration of the indicator, which generally is host antibodies and its short half-life. However, this technique may serve as a convenient pre-screening test for detecting the acute COVID-19 disease. On the other hand, the direct detection of this virus through the identification of its cell surface proteins (Approach 2)

* Corresponding authors at: Advanced Membrane Technology Research Centre, Universiti Teknologi Malaysia (UTM), 81310 Johor Bahru, Malaysia (A. Samavati).
E-mail addresses: salireza@utm.my (A. Samavati), afauzi@utm.my (A. Fauzi Ismail).

https://doi.org/10.1016/j.cej.2020.127655
Received 14 July 2020; Received in revised form 19 September 2020; Accepted 22 September 2020
Available online 10 November 2020
1385-8947/© 2020 Elsevier B.V. All rights reserved.

and unique antigen is practical. The COVID-19 virus has a small size of 65–125 nm in diameter [6]. This enveloped RNA virus is monopartite and linear with a comparatively large and positive sense ssRNA genome of 27–32 kb in size, which is the largest among all RNA virus genomes [7]. It consists of five structural proteins, i.e., membrane glycoprotein (M), spike glycoprotein (S), nucleocapsid interrupt phosphoprotein (N), envelope protein (E), and hemagglutinin-esterase glycoprotein (HE) in addition to two nonstructural polyprotein precursors of polyprotein1a ((pp1a) and polyprotein 1ab (pp1ab) [8]. The spike surface protein composition consists of the carboxylic acid group (—COOH) and amine group (—NH_2), which play an essential role in binding the virus to the host cell receptors.

Nowadays, miniaturized Au/fiber Bragg grating (FBG) probe due to its immunity to electromagnetic interferences, high sensitivity, and capacity for portable usage is a promising device in sensing and biosensing applications [9,10]. FBG is also used as an immunosensor for real-time detection of E. coli bacteria as well as temperature, pressure, strain, and humidity [11]. When the total internal reflection of light occurs in the core-cladding interface of optical fiber, a part of guided wave energy is leaked into the cladding, which is called evanescent wave. The surrounding refractive index has a major influence on evanescent wave, and this wave is very sensitive to any changes that occur in the refractive index of analyte liquids. This feature is utilized to develop evanescent-based optic fiber sensors. In order to assist the evanescent wave to penetrate into the surrounding medium, a certain portion of the fiber cladding on the grating area of the fiber needs to be removed [12].

The coherent oscillation of free electrons at the boundary of the metal-dielectric interface is called surface plasmon resonance (SPR) that is categorized into two groups: propagating surface plasmon and localized surface plasmon. The former waves propagate on the flat metal-dielectric interface, while the later waves occur due to conduction electrons oscillation. When the resonance condition is satisfied, it gives progress to large extinction coefficients. The peak wavelength, amplitude, and width of SPR depend on the metal layer composition, separation distance, size, shape, and dielectric surrounding environment of the nanolayer [13,14]. SPR-based biochemical sensors using optical fiber have been used in the research of Guangyu Qiu et al. [15]. The fabricated sensor in their study combines two different effects of optical and thermal for safe and reliable detection of the virus. In their research, a tiny gold nanostructure was deposited on a glass substrate as a sensing part; then, DNA receptors are artificially produced, which are matched with the specific RNA sequences of the SARS-CoV-2 as a measurand media exposed to the sensing part. When the virus molecules with unique RNA bind to the surface, due to the changes that occur to the local refractive index, the excited plasmonic near-field is altered. As a result, the virus can be identified through considering these changes [15].

To distinguish the new coronavirus and bring the pandemic under control, immediate and consistent tests are instantly demanded. In case of respiratory infections, the majority of laboratories use a reverse transcription polymerase chain reaction (RT-PCR) for a short time, which is a molecular method to detect viruses. These methods are well established and able to detect even small quantity of virus; on the other hand, they are time consuming and prone to error, and clinicians are at higher risk for tracing the virus from infected patients. Therefore, our fabricated highly sensitive FBG optical fiber sensor is proposed to detect the COVID-19 virus accurately with the capability to provide a remote sensor device. Moreover, the fabrication process of our sensor is also cost effective and the total expenses is less than 25 $. To the best of our knowledge, this is the first modified FBG sensor that directly detects the COVID-19 virus through patient saliva. A variety of microscopic and spectroscopic characterization techniques are employed to examine the sensor structure and evaluate its performance in identifying the infected patients through saliva testing.

2. Experiment

2.1. Fabrication of FBG

A single-mode glass optical fiber, having core and cladding diameters of 8.2 μm and 125 μm, respectively, with the grating length of 10 mm is utilized to prepare FBG. The operational wavelength of FBG was 1547 nm which was determined based on the maximum amplitude of broadband light source that appeared at that specific wavelength. The cladding and core refractive index were 1.4500 ± 0.0025 and 1.4765 ± 0.0025, respectively. The cladding material was silica doped by fluorine and the core material was silica. The photo-imprints pattern via an excimer laser was used to modulate the core refractive index of the fiber and create the grating pattern along with the fiber. The Lambda Physik, Germany; Model Compex 110 excimer laser in the order of ± 1 beam operated at 193 nm wavelength, 50 Hz, 100 mJ, and 10 ns pulses duration was utilized in this study. The phase mask grating corrugation period was 1072.6 nm. To complete the Bragg grating inscription, the fiber was exposed to intense UV light for 300 s.

2.2. FBG modification for COVID-19 virus identification

To prepare a highly sensitive fiber probe for virus detection, the following procedures are carried out. Initially, the majority of FBG cladding needs to be detached; however, the removing procedure should not damage the core surface. Any corrosion in the core surface can interrupt the total internal reflection and lower the probe efficiency. Therefore, when the FBG fiber was immersed in a 30% HF solution at 15 °C for removing the cladding part, the light transmission intensity was dynamically monitored. Then, at the optimum time, when the total internal reflection was not affected yet, the removing process was stopped. The rate of etching was ~ 1.06 μm/min. Then, the unclad part was subject to coating with Au nanolayer and decorating with graphene oxide (GO). The sputtering technique was used to deposit the Au nanolayer of the unclad FBG. The argon pressure and sputtering time were set to 0.1 mbar and 150 s, respectively. The sputtering current was fixed at 50 mA, and to ensure homogeneous coating on both sides, FBG was rotated 180° during the deposition process. After the deposition of the Au nanolayer, the final sensor fabrication phase was to decorate the sensing part with graphene oxide (GO), which is explained below.

Simplified Hummers' method was employed to synthesize GO [16]. The drop-casting technique was employed to deposit the GO nanostructured onto the Au coated FBG sensor. Initially, the graphene with concentrations of 0.005 mg/l was dissolved in methanol. The 5 μl of the solution was then dripped onto the Au-coated FBG fiber and left to dry. After the evaporation of the methanol, a layer of graphene was formed on the probe. A mixture of 400 μM EDC (1-ethyl-3-(3-dimethylaminopropyl)carbodiimide hydrochloride)/100 μM NHS (N-hydroxysuccinimide) at a volume ratio of 1:1 was provided in order to activate the carboxyl end groups on the surface of GO sheets to form a covalent bond and immobilize the hydrocarbon chains. Then, the FBG probe was post-annealed at 70 °C for 30 min. Finally, the probe was allowed to cool down in a dry cabinet before being used. For the morphological, structural, and chemical composition study of the GO decorated Au/FBG probe, a similar drop-casting method was replicated on a glass substrate coated with Au layer using a procedure similar to that of the FBG probe fabrication.

2.3. Saliva collection and virus quantification

In this study, 4 male and 2 female patients with the average age of 56.5 years (ranging from 34 to 71 years), who showed positive salivary infectious at different stages of diseases (early infection phase, pulmonary phase, and hyperinflammatory phase), were subject to saliva collection using the Norgeńs saliva RNA collection and preservation devices. It is worth noting that all patients were still hospitalized at the

time of writing this paper. Viral RNA was isolated from aliquots of saliva from the patients by means of the QIAamp viral RNA mini kit (Qiagen, Hilden, Germany). The detection of the virus was carried out by a real-time RT-PCR. The density of COVID-19 viruses for the samples was found to be in the range of 1.6×10^3 copies/mL to 1.2×10^8 copies/mL. The samples were then tested using our fabricated sensor.

2.4. Experimental setup and fiber sensor characterization

Fig. 1 displays a diagram of the experiment setup for the identification of the COVID-19 virus. In the process of this study, the light source (FiberLabs Inc.) was connected into one of the input ports, and an optical spectral analyzer (Yokogawa AQ6374) was launched into the output port. The reflected light signal from the FBG probe after modulating by the analyte surrounding was detected using an optical analyzer. The patients' saliva with different COVID-19 virus densities was prepared as the analyte liquid. The saliva sterile container was fully covered to prevent any contact with outside media; it was placed in a temperature-controlled bath with an ambient temperature of 25° to avoid any temperature effect on the COVID-19 virus detection process. The wavelength and amplitude numbers were recorded after 10, 20, 50, 100, 200, 400, and 1600 s of exposing the patients' saliva to the probe. Before immersing the probe to another sample (saliva with different concentrations), the fiber probe was washed using distilled water, and it was let be dried for 30 min.

Field emission scanning electron microscope (FESEM, JEOLJSM 6380LA), which is attached with energy dispersive X-ray spectrometer (EDX), was used for morphological and elemental analysis of the probe. X-ray diffraction (XRD) via Bruker D8 Advance Diffractometer with Cu-Kα_1 radiations at 40Kv was employed for the structural study of the GO decorated Au/FBG probe. For chemical composition analysis, Fourier-transform infrared spectroscopy (FTIR) provided by Thermo Fisher Scientific Inc., USA, was used, and the atomic force microscopy (AFM -SPI3800) built by Seiko Instrument Inc. (SII) was utilized to observe the growth morphology of the coated materials.

3. Sensing mechanism

Fig. 2a and b schematically depict the sensing mechanism of our fabricated probe. The sensor fundamentals are based on the modulation of surface plasmon resonance wave by varying the surrounding refractive index. The spike glycoprotein (S) is the main target for the neutralization of antibody, binding the COVID virus with the receptor, and providing the virus entry through mediating the membrane fusion. As can be seen in the schematic diagram, this protein contains both

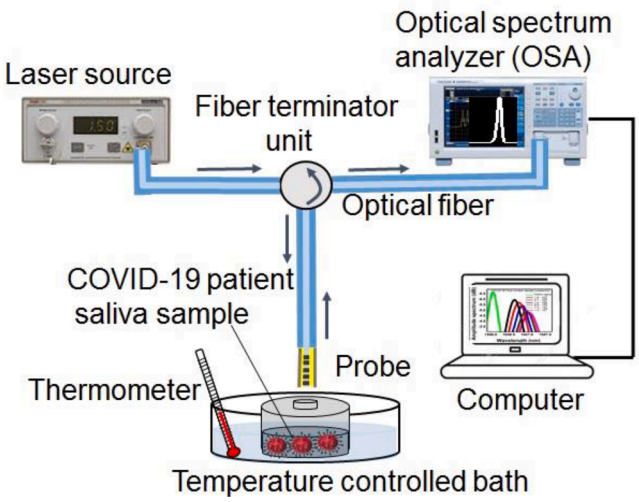

Fig. 1. Schematic diagram of the experimental setup.

carboxylic acid group (—COOH) and amine group (—NH_2). Moreover, GO possesses a number of carboxylic acid groups (—COOH) that can definitely bind with the free —NH2 terminals of the S protein at the presence of activating agents (EDC/NHS) and create the strong amide covalent linkage. Fig. 2b schematically illustrates the binding process of COVID-19 spike protein with the GO surface. EDC is coupled with NHS as a zero-length crosslinker to efficiently form conjugates between a COVID-19 S protein and a peptide at physiologic pH. It mediates crosslinking without becoming a part of the final amide bond between the spike protein and the carboxylic group in GO. Therefore, similar to most of the biological macromolecules, it is water soluble and can be dissolved in aqueous buffer solutions. Thus, the solubility of activation groups and their isourea by-product into the reaction medium allows easy purification of the crosslinked product with chromatography, precipitation, ultrafiltration, or dialysis and also verifies the *reusability* of the device. Moreover, large surface area and oxygen-rich functional groups on the surface of GO lead to high loading of S glycoprotein onto the sensing surface. From the other aspect, the existence of nano-level defects and 2D channels between the stacked GO nanosheets with an interlayer spacing of ~0.8 nm and 1.3 nm in a dry and aqueous environment, respectively, promotes a unique behavior towards patient saliva. It functions as a sieve and lets the water and other molecules penetrate through its membranes; however, it resists the COVID-19 virus with a considerably larger size and traps them on the surface of the GO layer. Therefore, the trapped viruses, which form an extra layer over the GO, change the surrounding refractive index of the sensor.

When a light wave reflected from FBG propagates in the core of the fiber, a part of the incident light on the Au film, in the form of non-uniform evanescent electromagnetic wave, transmits in the metal [17], which exponentially decays in a perpendicular direction to the cladding-Au interface. The evanescent wave penetrates across the Au film especially when the film is adequately thin (less than ~ 50 nm) and couples with a surface plasmon wave at the outer boundary of the film (see schematic diagram at Fig. 2) [18]. If the propagation constant of evanescent wave and surface plasmon are equal, the coupling between them is occurred.

Eq. (1) shows the wave vector of the plasmon wave (k_{sp}) [19]:

$$k_{sp} = \left(\frac{2\pi}{\lambda}\right)\sqrt{\frac{(n_{Au}^2 \times n_{GO}^2)}{(n_{Au}^2 + n_{GO}^2)}} \tag{1}$$

where the refractive index of Au and GO films are shown by n_{Au} and n_{GO}, respectively, and λ is the incident light wavelength. The SPR occurs when the relationship in Eq. (2) is satisfied, in which the energy transfers between the incident light and surface plasmon wave at the GO-Au interface.

$$n_p k_0 sin\theta_{sp} = k_{sp} = k_0\left[\frac{\varepsilon_{Au}\varepsilon_{GO}}{\varepsilon_{Au} + \varepsilon_{GO}}\right]^{1/2} \tag{2}$$

$K_0 = 2\pi/\lambda_0$ is the wave vector of an electromagnetic wave in vacuum, in which λ_0 is the wavelength in a vacuum. The ε_{Au} and ε_{GO} represent the dielectric constants of Au and GO layer, respectively. To fulfill the SPR condition, there are two possible ways: varying the wavelength of the light or varying the angle of incidence (θ). Wavelength interrogation, where SPR occurs as a dip intensity decrement at a certain wavelength, is used in a fiber optic SPR sensor. This feature enables the SPR phenomena to be exploited for sensing purposes. The Covid-19 infected patients' saliva, which acts as an analyte surrounding the probe and contains different quantities of viruses, is adsorbed on the Au film through the thin decorated GO layer, hence affecting the resonance conditions of the SPR sensor. The fiber optic SPR sensor performance is based on a spectral investigation. Equation (3) represents the transmission function of the detected light intensity by optical spectrum analyzer, which is normalized to the laser source power [20].

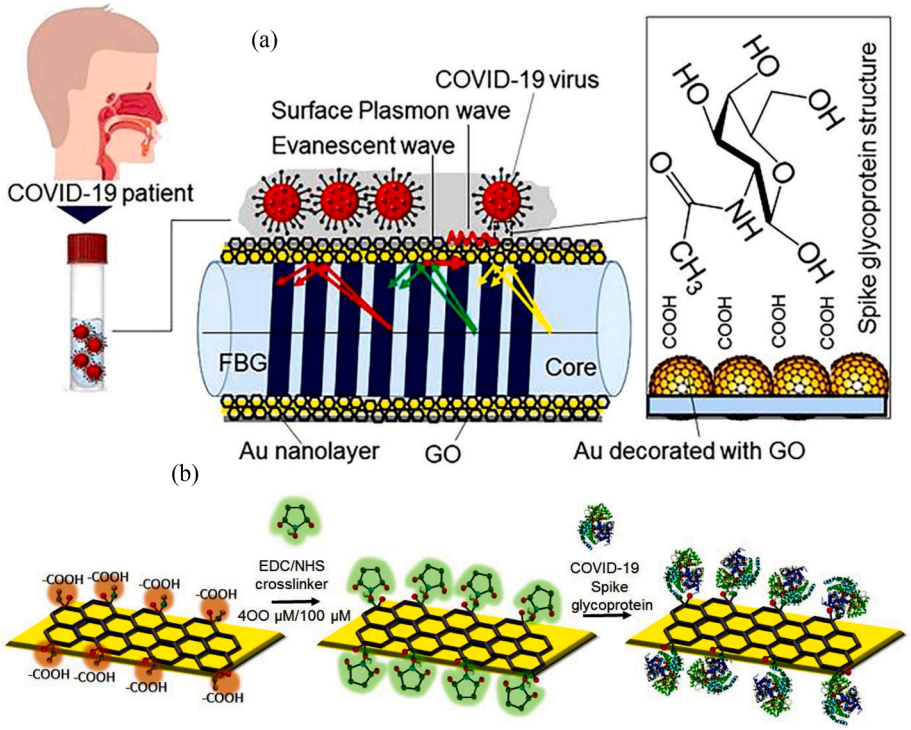

Fig. 2. Sensing mechanism diagram (a), binding of the spike glycoprotein of COVID-19 virus with activated GO using EDC/NHS (b).

$$Transmission(f) = \frac{\frac{1}{2}\int real\left(P(f)^{Monitor}\right)ds}{Lasers\ source\ power} = exp\left(-\frac{4\pi}{\lambda_0} imag(n_{eff})L\right) \quad (3)$$

where L is the sensing region length (1 mm), n_{eff} is the effective refractive index of the sensing region, which alters by varying the virus density in saliva as surrounding media, and λ_0 is the light source wavelength. The average power flow over the surface is obtained via integration of the Poynting vector P(f) respect to the surface normal S. At the SPR wavelength, the transmitted power or output intensity of the probe is dropped; as a result, with the use of this equation, the resonant wavelength of the probe can be derived. The intensity and wavelength sensitivity of the SPR sensor are presented as S_I and S_W, respectively, and given in Equation (4):

$$S_I = \frac{\Delta I_{res}}{\Delta\eta} S_w = \frac{\Delta\lambda_{res}}{\Delta\eta} \quad (4)$$

If the density of viruses (copies/mL) is varied by $\Delta\eta$, the resonance wavelength is shifted by $\Delta\lambda_{res}$, and the transmitted light amplitude is changed by ΔI_{res}.

4. Results and discussion

4.1. Probe analysis

The surface morphology of the prepared probe is shown in the FESEM images in Fig. 3a. The inset shows the AFM topographic image of the selected area. The GO-decorated Au nanolayer has an island structure with a dome-like shape. The cross-section FESEM image in Fig. 3b depicts the formation of 30 nm GO-decorated Au film on the unclad part of the FBG fiber. The EDX spectra presented as an inset in Fig. 3b consists of C, O, Si, and Au signals and confirms the formation of both GO and Au nanolayer on top of the unclad FBG fiber.

The crystal structure of GO/Au/glass substrate is characterized using the XRD technique, and its corresponding spectrum is shown in Fig. 4. The peaks at 2θ of 22.08◦ assign to (002) miler index of the hexagonal GO structure, which is paired with JCPDS number of 75-2078. The Au characteristic peaks occur at 2θ of 38.42◦, 44.50◦, 64.81◦, and 77.82◦ corresponding to indices of (111), (200), (220), and (311), respectively, which is in good agreement with standard JCPDS no. 04-0874

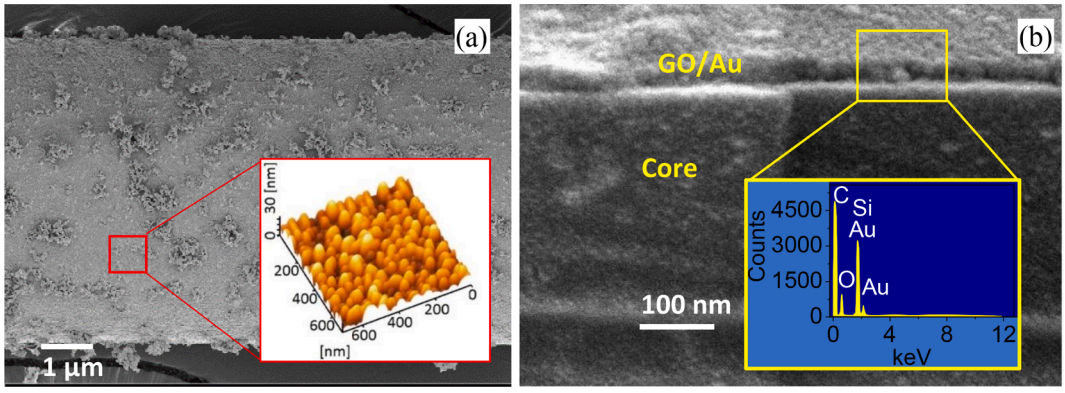

Fig. 3. The cross-sectional FESEM micrograph of the GO-decorated Au/FBG probe, inset illustrates the EDX spectra of the selected area (a) and top view of coated FBG, inset depicts the three-dimension AFM topographic image of the selected area (b).

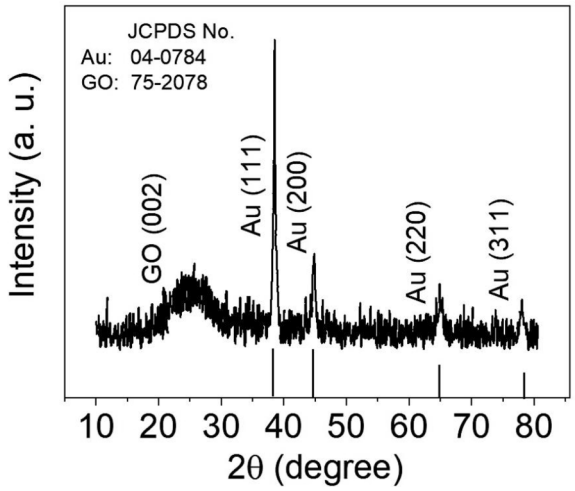

Fig. 4. The XRD pattern of the standard JCPDS file of the fcc phase of Au crystal (JCPDS no. 04-0784) and as-prepared GO/Au/glass plate.

pattern for Au. Moreover, the broadening of the diffraction peaks implies that the crystalline size of Au is relatively small. The crystallite size is calculated by the XRD patterns using the Debye Scherrer's formula [21]:

$$cos\theta = \frac{\lambda k}{D}\left(\frac{1}{\beta_D}\right) \quad (5)$$

where D is the crystallite size in nanometers, λ denotes the wavelength of the radiation (1.54056 Å for Cu Ka radiation), k is a constant that equals 0.94, β_D signifies the peak width at half-maximum intensity, and θ represents the highest intensity (1 1 1) peak position. The crystallite size is estimated to be 7.2 nm.

The sharp diffraction peak of the Au (1 1 1) with higher intensity shows that the growth of Au nanolayer during synthesis occurs at the lowest energy (1 1 1) facet. The Scherer equation was used to estimate the crystalline size of GO-coated Au/glass, and it was calculated to be 27.5 nm. This value is consistent with the observation from the AFM topographic image presented as an inset in Fig. 3b.

The functional groups in GO-coated Au/glass are analyzed using the FT-IR spectroscopy; the corresponding spectra are presented in Fig. 5. The FT-IR spectrum of the sample revealed a characteristic peak at around 3420 cm^{-1} matching with O—H bond, originated from the intercalated water molecules and —COOH group, which indicates the

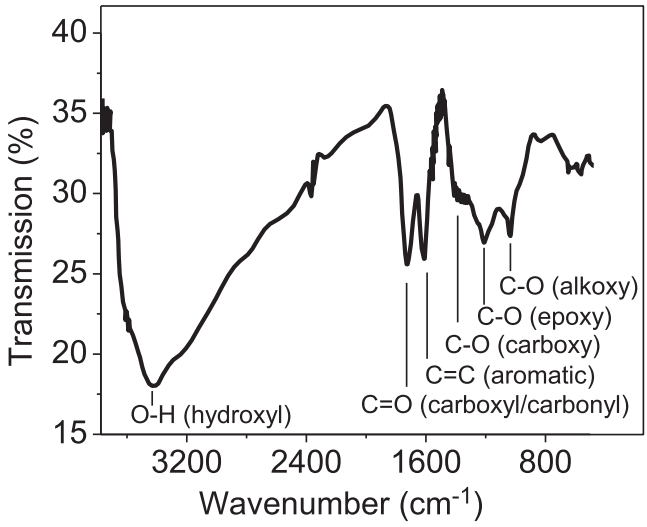

Fig. 5. FTIR spectra of GO coated Au/glass substrate.

possibility of amide bond formation of NH-GO once the probe is exposed to the patients' saliva. The signal at 1736 cm^{-1} corresponds to C═O stretching frequencies. The peaks created from aromatic C═C bending, phenolic C—O stretching, and epoxy C—O—C stretching are identified at 1637 cm^{-1}, 1222 cm^{-1}, and 1050 cm^{-1}, respectively. The expanded GO surface with oxygenated functional groups provides an effective nucleation and binding sites for the probe surface.

4.2. The SPR feature of the probe

Fig. 6a represents the spectra at the reflection port for bare FBG (partially un-cladded), FBG coated with 30 nm Au film, and Au/FBG probe decorated with GO. As depicted in the spectra, the amplitude of the reflected FBG spectra dropped drastically when the Au nanolayer-coated FBG was decorated with GO. In case of coated FBG, the coupling resonance between the surface plasmon wave on the metal film, which happens on the metal-dielectric interface and p-polarized electromagnetic (TM polarized) wave, is responsible for a rapid reduction of reflected light amplitude and represents the formation of SPR on the fabricated probe. The Au/FBG decorated with the GO sample was then exposed to three different analytes of air, distilled water, and healthy saliva; the reflected FBG signals are depicted in Fig. 6b. Inset figure summaries the peak wavelength changes and intensity deviation of the sensor with the change of external measurand. As can be seen in Fig. 6b, from air to healthy saliva, the FBG wavelength is shifted to red and the intensity is decreased. The SPR phenomenon is sensitive to the external refractive index; therefore, any change to the external refractive promotes an obvious deviation of the resonance. This, in turn, results in altering the FBG signal location and intensity. These results indicate that both wavelength and intensity interrogation can be utilized as sensing elements in our fabricated FBG optical fiber SPR sensor.

4.3. The probe functionality against the COVID-19 virus

Fig. 7 depicts the FBG probe amplitude and wavelength, subject to increasing the density of viruses in saliva at four different times of probe exposure to saliva. Both the amplitude and the wavelength variations of the resonance were obviously observed for all virus densities. For better comparison, the wavelength and intensity variation versus virus concentration at different reading times (from 10 s to 1600 s) are plotted separately in Fig. 8a and b, respectively. Increasing the virus density led to the formation of a thicker layer trapped over GO, which resulted in significant changes in the refractive index of the surrounding sensor in terms of the quantity of virus involved. Consequently, as mentioned in the sensing mechanism part, it altered the wavelength and intensity more significantly. For instance, in case of the saliva taken from a patient who is in the hyperinflammatory phase of the disease with 1.2×10^8 copies/mL virus concentration after 10 s of exposure time, the wavelength shifts and amplitude variance were 0.92 nm and 1.68 dB, respectively. However, these values for a patient in the early infection stage with 1.6×10^3 copies/mL virus concentration, were 0.39 nm and 0.48 dB, respectively.

From another perspective, by increasing the sensor exposing time to the virus, more bonds between —COOH of GO and NH group of virus spike glycoprotein occurred, which led to the formation of a thicker layer trapped over GO and also a change to the plasmon resonance wavelength pattern. Fig. 9a and b depict the variation in the wavelength and intensity of the signals due to SPR of the sensor for various COVID-19 densities as a function of probe exposing time to saliva. The healthy saliva is considered as measurand analyte, and the recorded wavelength and intensity at different exposing times are plotted as well. An approximately constant line with standard deviation of ±0.02 dB and ±0.01 nm for wavelength and intensity, respectively, was achieved. The wavelength shift and intensity variation were found more prominent at higher exposure times. However, after few hundred seconds, the rate of bond formation on the surface of GO became slower, which was due to a

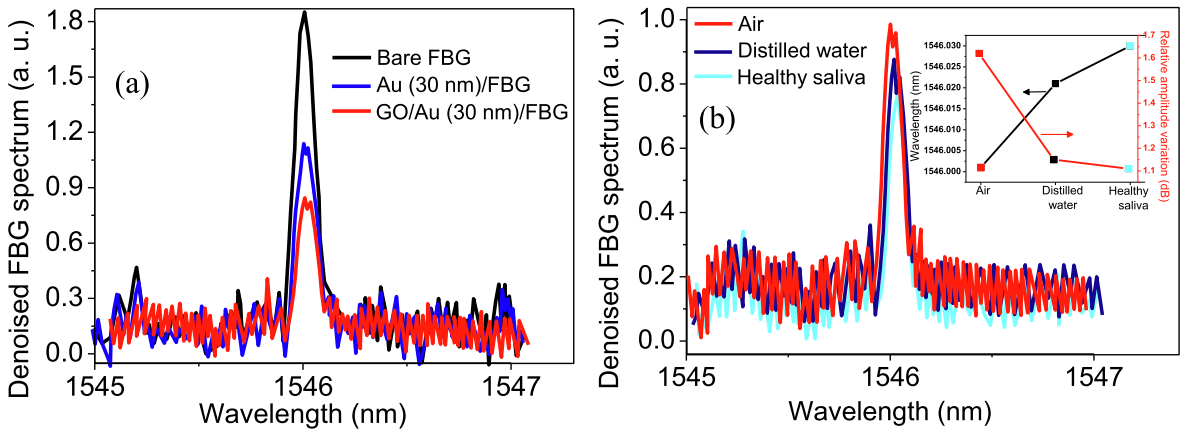

Fig. 6. Effect of 30 nm-thick Au and GO-decorated Au (30 nm) partially coated on unclad FBG spectra. Different amplitudes obtained are due to SPR of the coated layers (a), The detected spectra of GO decorated Au/FBG probe when exposes to air, distilled water, and healthy saliva. The inset shows the wavelength and intensity changes of the probe (b).

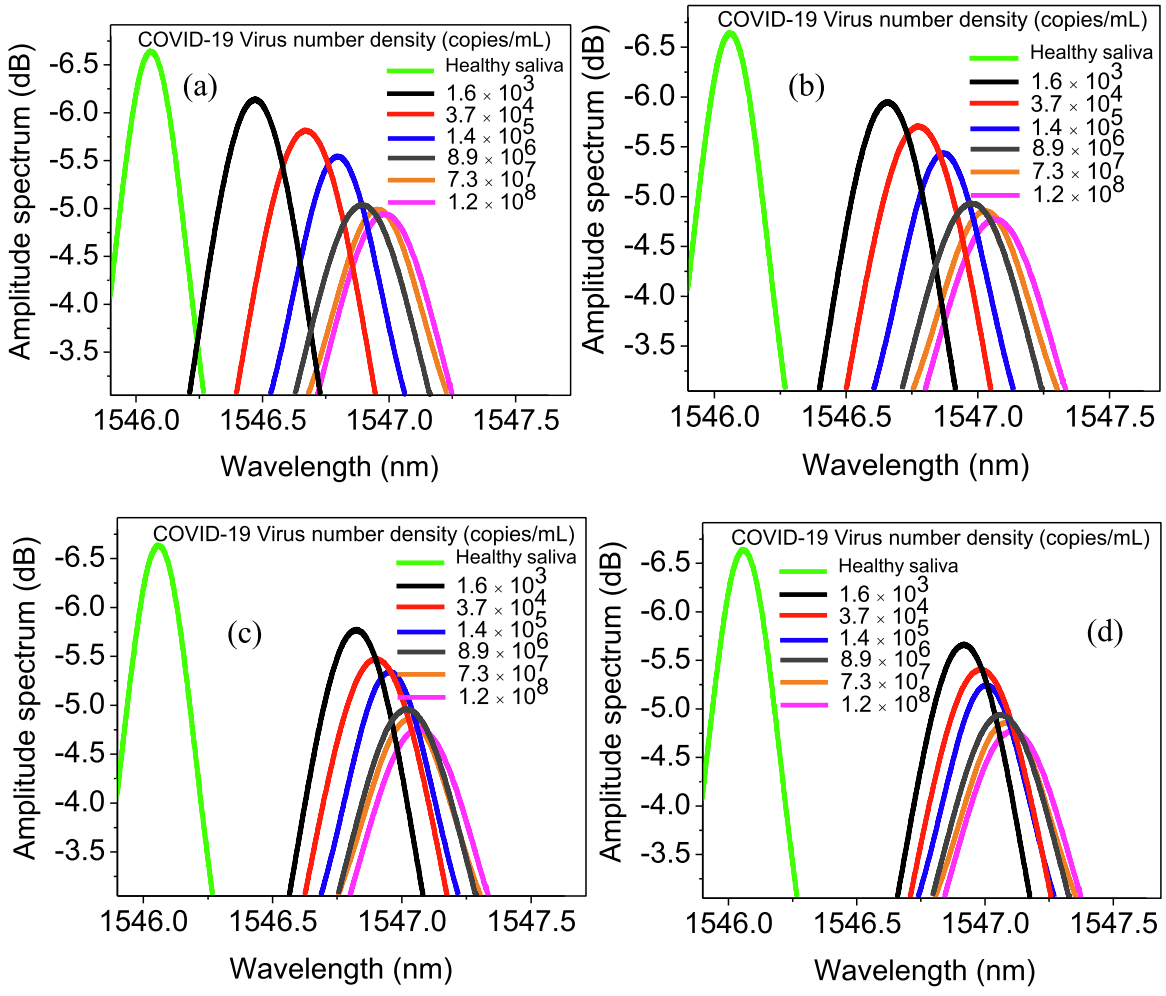

Fig. 7. GO-decorated Au/FBG probe spectra once immersed at different densities of COVID-19 virus after 10 sec (a), 20 sec (b), 50 sec (c), and 100 sec (d).

lack of enough free activated nucleation site on the GO surface that was mostly occupied by another virus spike. After 400 s, the wavelength and intensity changes were not significant compared to shorter exposure times. As can be seen in both Fig. 9a and b, the deviation from healthy saliva increased when the virus density increased. Initially, the deviation increased exponentially; after 200 s, it became constant. Consequently, this method of detection not only can be used to distinguish the infected patients from non-infected ones, but also can determine the level of illness through patients' saliva. Moreover, the results revealed that the rapid diagnosis of the COVID-19 virus within 10 s would be possible by our proposed sensor. Eq. (4) was used to calculate the wavelength and intensity sensitivity against virus density in the saliva; the summarized results are presented in Table 1. As it was expected, by passing the exposure time, the sensitivity of the probe decreased due to the

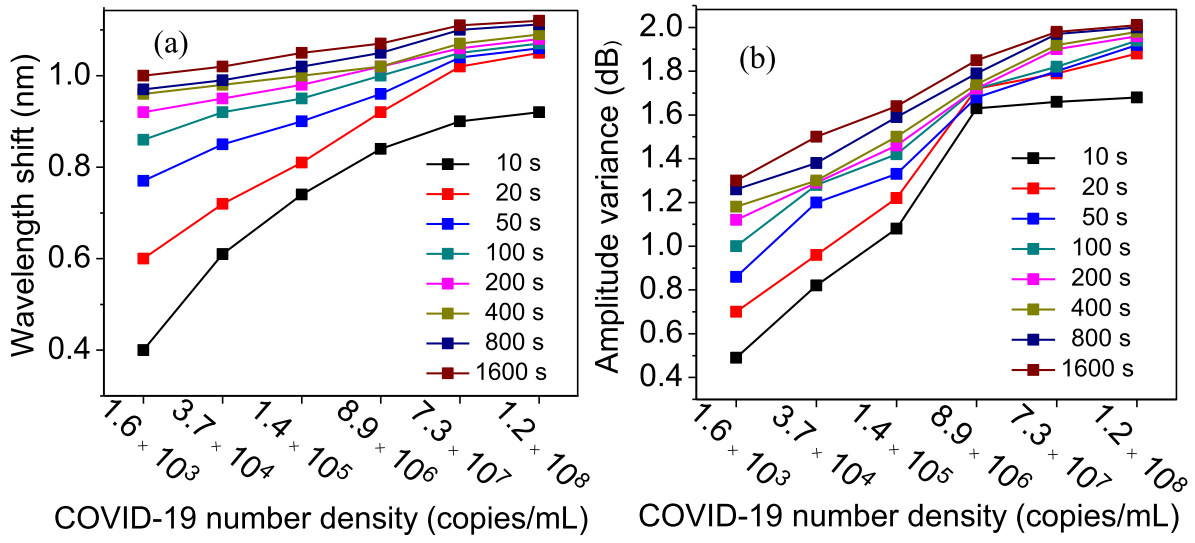

Fig. 8. The wavelength shifts (a) and intensity changes (b) of the detected light once it passes through the fiber probe as a function of virus number density (concentration in saliva) at different exposure times.

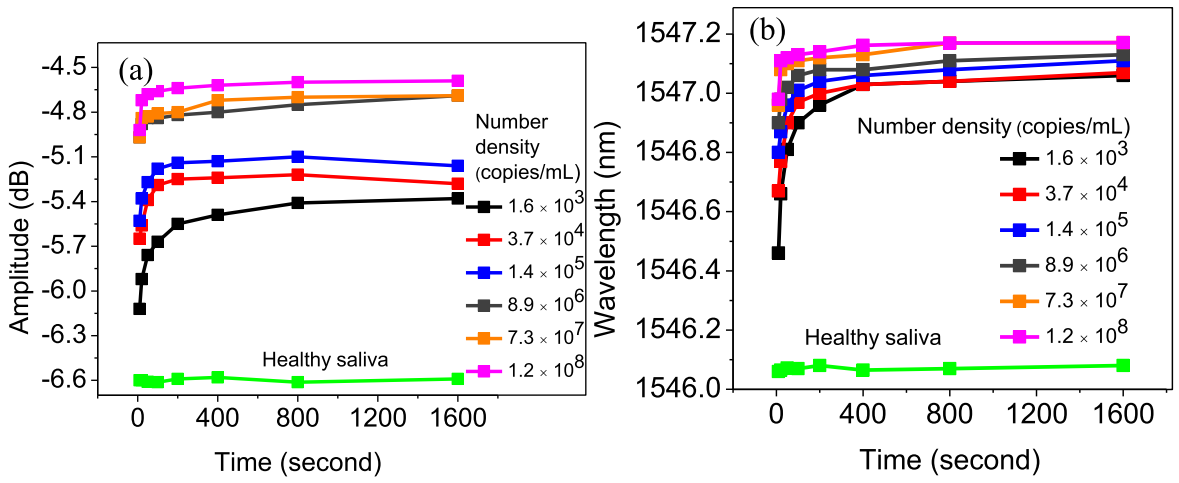

Fig. 9. The wavelength (a) and intensity (b) value of detected light once it passes through the fiber probe as a function of exposing time for different virus concentrations. The plot for healthy saliva can be used as reference, and deviation from that reveals the patient's infection level.

Table 1
Wavelength and intensity sensitivity of fabricated sensor against virus density in saliva.

Exposing time (sec)	Wavelength sensitivity × 10^{-8} (nm/virus number)	Amplitude sensitivity × 10^{-8} (dB/virus number)
10	0.4250	1.0008
20	0.3666	0.9750
50	0.2416	0.8666
100	0.1916	0.8083
200	0.1166	0.6750
400	0.1150	0.6500
800	0.1000	0.6167
1600	0.0833	0.5666

occupation of activated and binding sites existing on the surface of GO.

5. Conclusion

In this study, an Au/FBG probe decorated with GO was fabricated and its sensitivity against different COVID-19 concentrations in patients' saliva was experimentally demonstrated. The use of saliva as an analyte sample has several advantages, e.g., an easier and more comfortable collecting process compared to swab, reducing the risk to health care workers, and reducing the consumption of personal protective equipment. These advantages motivated us to try the diagnosis of the infected saliva through monitoring the FBG probe responses against the COVID-19 virus. In the experiments, the fabricated probe showed an instant response to patients' saliva even at the early stages of infection. After 10 s of exposing the probe to patients' saliva in the early stage of disease (1.6×10^3 copies/mL), the wavelength and intensity of detected light were modulated for 0.39 nm and 0.49 dB, respectively. The deviation of wavelength and intensity of light from the healthy saliva exponentially increased beyond 200 s and became approximately constant after that time. The use of an accurate, sensitive, and reliable sensor with a fast response to the COVID-19 virus in the patients' saliva with the capability of remote sensing features makes the fabricated probe a promising candidate for diagnosing the virus, hence controlling the pandemic.

Declaration of Competing Interest

The authors declare that they have no known competing financial interests or personal relationships that could have appeared to influence

the work reported in this paper.

Acknowledgments

This study is supported by Universiti Teknologi Malaysia via vote number R.J130000.7609.4C112 and Arak university Iran. The authors would also like to thank Intensive Care Unit, Sina hospital, Hamadan, Iran for the technical support.

References

[1] N.C. Who, Situation Report 50, WHO, 2020.
[2] M. Coccia, Factors determining the diffusion of COVID-19 and suggested strategy to prevent future accelerated viral infectivity similar to COVID, Sci. Total Environ. (2020), 138474.
[3] A.R. Sahin, A. Erdogan, P.M. Agaoglu, Y. Dineri, A.Y. Cakirci, M.E. Senel, R. A. Okyay, A.M. Tasdogan, novel coronavirus (COVID-19) outbreak: a review of the current literature, EJMO 4 (2020) (2019) 1–7.
[4] X. Peng, X. Xu, Y. Li, L. Cheng, X. Zhou, B. Ren, Transmission routes of 2019-nCoV and controls in dental practice, Int. J. Oral Sci. 12 (2020) 1–6.
[5] D. Vinayachandran, B. Saravanakarthikeyan, Salivary diagnostics in COVID-19: Future research implications, J. Dental Sci. (2020).
[6] M.A. Shereen, S. Khan, A. Kazmi, N. Bashir, R. Siddique, COVID-19 infection: Origin, transmission, and characteristics of human coronaviruses, J. Adv. Res. (2020).
[7] X. Li, M. Geng, Y. Peng, L. Meng, S. Lu, Molecular immune pathogenesis and diagnosis of COVID-19, J. Pharm. Anal. (2020).
[8] S. Perlman, J. Netland, Coronaviruses post-SARS: update on replication and pathogenesis, Nat. Rev. Microbiol. 7 (2009) 439–450.
[9] A. Samavati, Z. Samavati, A.F. Ismail, N. Yahya, M. Othman, M. Rahman, M. Bakar, K. Koo, M. Salebi, I.S. Amiri, An FBG magnetic sensor for oil flow monitoring in sandstone core, RSC Adv. 9 (2019) 35878–35886.
[10] S. Bandyopadhyay, L. Shao, C. Wang, S. Liu, Q. Wu, G. Gu, J. Hu, Y. Liu, X. Chen, Z. Song, Study on optimization of nano-coatings for ultra-sensitive biosensors based on long-period fiber grating, Sens. Bio-Sens. Res. 27 (2020), 100320.
[11] C. Caucheteur, M. Loyez, M. Lobry, R. Wattiez, Biofunctionalization strategies for optical fiber grating immunosensors, Biophotonics in Point-of-Care, Int. Soc. Opt. Photonics (2020) 1136109.
[12] Z. Samavati, A. Samavati, A.F. Ismail, N. Yahya, M.A. Rahman, M.H.D. Othman, Effect of acetone/methanol ratio as a hybrid solvent on fabrication of polymethylmethacrylate optical fiber sensor, Opt. Laser Technol. 123 (2020), 105896.
[13] A.N. Emam, A.S. Mansour, M.B. Mohamed, G.G. Mohamed, Plasmonic Hybrid Nanocomposites for Plasmon-Enhanced Fluorescence and Their Biomedical Applications, Nanosci. Med. 1 (2020) 459–488.
[14] R. Shyamala, L.N. Gomathi Devi, Surface plasmon resonance effect of Ag metallized SnO2 particles: Exploration of metal induced gap states and characteristic properties of Ohmic junction, Surf. Interface Anal. 52 (2020) 374–385.
[15] G. Qiu, Z. Gai, Y. Tao, J. Schmitt, G.A. Kullak-Ublick, J. Wang, Dual-functional plasmonic photothermal biosensors for highly accurate severe acute respiratory syndrome coronavirus 2 detection, ACS Nano 14 (2020) 5268–5277.
[16] W.S. Hummers Jr, R.E. Offeman, Preparation of graphitic oxide, J. Am. Chem. Soc. 80 (1958) 1339.
[17] Z. Samavati, A. Samavati, A.F. Ismail, M.H.D. Othman, M.A. Rahman, Comprehensive investigation of evanescent wave optical fiber refractive index sensor coated with ZnO nanoparticles, Opt. Fiber Technol. 52 (2019), 101976.
[18] H. Raether, Surface plasmons on smooth surfaces, in: Surface plasmons on smooth and rough surfaces and on gratings, Springer, Berlin, Heidelberg, 1988, pp. 4–39.
[19] R.K. Verma, Sensitivity enhancement of a lossy mode resonance based tapered fiber optic sensor with an optimum taper profile, J. Phys. D Appl. Phys. 51 (41) (2018), 415302.
[20] P.T. Arasu, A.S.M. Noor, A.A. Shabaneh, M.H. Yaacob, H.N. Lim, M.A. Mahdi, Fiber Bragg grating assisted surface plasmon resonance sensor with graphene oxide sensing layer, Opt. Commun. 380 (2016) 260–266.
[21] B.D. Cullity, Elements of X-ray Diffraction, Addison-Wesley Publishing, 1956.